2011 American Control Conference
on O'Farrell Street, San Francisco, CA, USA
June 29 - July 01, 2011

LIDAR-based FX-RLS Feedforward Control For Wind Turbine Load Mitigation

Na Wang, Kathryn E. Johnson
Division of Engineering, Colorado School of Mines, Golden, CO, 80401, USA
and Alan D. Wright
US National Renewable Energy Laboratory, Golden, CO, 80401, USA

***Abstract*— An adaptive feedforward controller based on a filtered-x recursive least square (FX-RLS) algorithm and a non-adaptive feedforward controller based on a zero-phase-error tracking control (ZPETC) technique have been designed to augment a collective pitch proportional-integral (PI) feedback controller for wind turbine rotor speed regulation and component load reduction when the turbine is operating in above rated wind speed. The feedforward controllers use wind speed measurements provided by a commercial light detection and ranging (LIDAR) system. Simulations show that augmenting the baseline PI feedback control with ZPETC feedforward control improves the blade loads but worsens the tower loads. The FX-RLS feedforward algorithm gives better performance than both the baseline PI feedback and the ZPETC feedforward in both tower (fore-aft and side-to-side) and blade (flapwise and edgewise) bending moment mitigation, even with a realistic 1 Hz LIDAR data update rate.**

I. Introduction

Many advanced control techniques for wind turbine fatigue load alleviation have been developed recently. Most are linear non-adaptive feedback control techniques, such as proportional-integral (PI) control, full-state feedback control, disturbance accommodating control (DAC), and linear quadratic regulators (LQR) [1], [2]. These linear controllers are usually designed for one specific operating point, so performance may degrade when the wind turbine operates away from that operating point. However, wind turbines are highly nonlinear, so nonlinear and adaptive techniques may further improve performance. Gain scheduling techniques such as [3] can improve operation over a range of operating points but have limitations in implementation [4]. Until very recently, high-bandwidth accurate wind speed measurements for use in wind turbine control were not realistically obtainable, though averages over tens of minutes or longer were sometimes achievable. Recent advances in light detection and ranging (LIDAR) systems and significant decreases in unit prices have led to interest in using them to obtain real-time measurements of wind speed or direction inputs local to individual wind turbines [5], opening a new area of research in the area of feedforward wind turbine control. PI feedback controller have been augmented with various collective pitch and individual pitch feedforward controllers using gain-scheduled model-inverse and gain-scheduled shaped compensator, showing promising results [6]. However, these linear feedforward controllers may not reject disturbances effectively over the entire range of wind turbine operating points.

Adaptive control has the potential to overcome some of the drawbacks of linear time-invariant control, in this case because the control law can be updated at every time step according to the wind input conditions and information from the turbine. Adaptive feedforward control can help disturbance rejection and vibration suppression for aircraft [7], and similar techniques may be beneficial for wind turbines when combined with LIDAR. Ultimately it is hoped that these advanced control strategies will reduce the cost of wind energy, either by extending the lifetime of a wind turbine or by allowing it to be built more inexpensively initially.

In this paper, we describe an adaptive filtered-x recursive least square (FX-RLS) feedforward controller developed for use in conjunction with a LIDAR with various assumed capabilities (from currently available commercially to what might be available in a few years). For comparison, we also describe and simulate a zero-phase-error tracking control (ZPETC) [8] feedforward controller. According to the simulation results, in the presence of the wind speed preview measurements enabled by the LIDAR sensor, the FX-RLS controller performs better than the baseline feedback-only and the ZPETC feedforward controllers in both structural load reduction and rotor speed tracking when the wind turbine is operating in region 3, the operational regime during which the turbine limits power and the wind speed is above rated.

The remainder of this paper is organized as follows. Section II presents the wind turbine model and its control structure. Section III describes the simulated wind turbine model, LIDAR code model, and turbulent wind field respectively. Section IV introduces the design of non-adaptive and adaptive feedforward controllers. Section V gives the simulation results compared with a PI feedback only controller. Finally, concluding remarks are given in Section VI.

II. Turbine Description

The turbine modeled for this research is the 600 kW, three-bladed, horizontal-axis controls advanced research turbine

Graduate student, Division of Engineering, Colorado School of Mines, Golden, CO.
Clare Boothe Luce Assistant Professor, Division of Engineering, Colorado School of Mines, Golden, CO.
Senior Engineer, National Wind Technology Center, NREL, Golden, CO

(CART3) at the National Renewable Energy Laboratory's (NREL) National Wind Technology Center. CART3 is capable of full range variable speed operation and full-span individual blade pitch [9]. CART3 has a hub height of 34.7 m, a rotor diameter of 40 m, a rated generator torque of 3524 kN*m, a rated rotor speed of 41.7 rpm, a rated rotor power of 667 kW, and a maximum pitch rate of 18 deg/sec. Though CART3 is smaller than modern utiliy-scale turbines, this simulation study was performed in preparation for field tests on this turbine.

Though the details of modern utility-scale turbine control algorithms are proprietary and closely protected by industry, until recently most were straightforward PI-based collective blade pitch feedback controllers. These controllers typically operate on an input signal such as the error in rotor speed (or power) when the turbine is operating above rated wind speed. More details about the PI feedback-only collective pitch controller and used as a baseline controller in this study is given in [10]. Our research augments the feedback only strategy with a feedfoward path, as shown in Fig. 1, as will be described in Section IV.

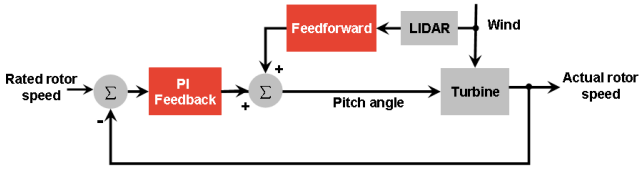

Fig. 1. Combined PI feedback and feedforward control [6].

III. Simulation Description

In this section, we introduce the simulation environment used in this research, which includes the CART3 turbine model, the LIDAR device model, and the turbulent wind fields used in the simulation tests.

A. Simulated turbine model

All simulations are performed using a full non-linear turbine model provided by the FAST software [11]. FAST can be used to model two and three bladed horizontal-axis wind turbines. FAST allows many degrees of freedom (DOFs) to be turned on or off; in our research, we enabled the following 16 DOFs: generator (1 DOF), drive train (1 DOF), 1st and 2nd blade flapwise mode (2×3 DOFs), 1st blade edgewise mode (1×3 DOFs), 1st and 2nd tower fore-aft mode (2 DOFs), 1st and 2nd tower side-to-side mode (2 DOFs) and yaw (1 DOF). The default FAST tool does not include a pitch actuator model, but one can be incorporated into the simulation within the Simulink environment. To avoid unattainable pitch rate control signals, used a 1st-order low-pass filter (LPF) with 60 rad/s corner frequency. FAST can also be used to linearize the turbine at various operating points to obtain models useful for control design.

B. LIDAR code

The feedforward controllers require wind speed measurements upwind of the turbine. In this research, we model a continuous wave (CW) coherent Doppler LIDAR mounted in a turbine hub, which allows it to scan a circle in front of the turbine. These LIDAR measurements have been incorporated into FAST as described in [12]. By setting the preview time for the wind speed measurement in the simulation, the LIDAR code can provide measurements at a certain distance, a function of wind speed, in front of the entire rotor. In initial simulations the LIDAR simulator provides perfect measurements at up to 100 Hz, which is the sampling rate of the wind turbine controller. However, our research also examines the effects of slower, more realistic LIDAR measurement rates down to 1 Hz.

C. Simulated Wind file

A TurbSim-generated [13] wind input file is used as turbulent wind field for the simulations shown in this paper, with a hub height mean wind speed of 18 m/s, a vertical stability parameter Ri_{TL} of 0.043, a vertical power law shear exponent α_D of 0.125, and a mean friction velocity of 0.688 m/s. TurbSim is a stochastic, full-field, turbulent wind simulator developed by NREL. It uses a statistical model to numerically simulate the time series of three component wind speed vectors at points in a two-dimensional vertical rectangular grid. Turbsim wind conditions march forward in a frozen field toward the turbine; that is, the wind fields do not evolve with time.

IV. Feedforward Control Design

In this section, we describe two feedforward control strategies investigated in this research. The ZPETC algorithm is a model-inverse-based non-adaptive feedforward control, while the FX-RLS algorithm is adaptive. Both of the feedfoward controllers augment the same PI feedback collective pitch baseline controller when wind speed is above rated.

A. ZPETC Controller

To design the ZPETC feedforward controller, the first step is to obtain a linear model of wind turbine around a specific operating point, which we select at wind speed u_0 = 18 m/s, rotor speed Ω_0 = 41.7 rpm, and pitch angle β_0 = 12.8 degree. The wind turbine is linearized with five degrees of freedom enabled, including the first flapwise blade mode for all three blades and the drive train and generator DOFs. Two transfer functions are obtained to represent the linearized relationships between the pitch angle β and rotor speed error Ω_e ($P_{\Omega_e\beta}$) and the wind speed u and Ω_e ($P_{\Omega_e u}$), as shown in Fig. 2. The linear model-inverse feedforward controller F in Fig. 2 is used to cancel the effect of turbulence in wind speed u on deviations from the rotor speed error Ω_e. According to Fig. 2, we have

$$\Omega_e = \frac{P_{\Omega_e\beta} \cdot F \cdot u + P_{\Omega_e u} \cdot u}{1 - P_{\Omega_e\beta} \cdot FB}. \quad (1)$$

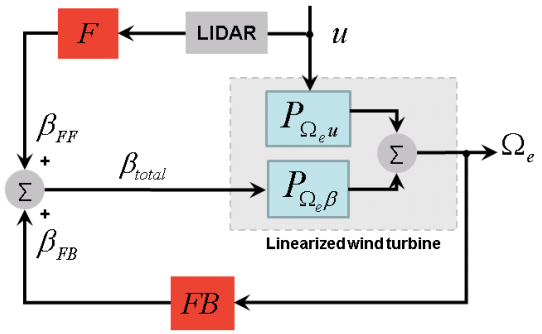

Fig. 2. Combined collective feedback and model-inverse-based feedforward control with linearized wind turbine model. Ω_e denotes the rotor speed error. The sum of the collective pitch command generated by the feedforward controller (F) and the baseline feedback controller (FB) is the input to the linearized turbine model.

Since the desired rotor speed error ($\Omega_{e(desired)}$) is zero, we can solve for the feedforward controller F by setting the numerator of (1) equal to zero. Then, we have

$$F = -P_{\Omega_e \beta}^{-1} \cdot P_{\Omega_e u}. \tag{2}$$

If $P_{\Omega_e \beta}$ contains non-minimum phase zeros, the resulting F is unstable. To avoid this situation, a stable model-inverse approximation is used instead. In this research, we apply the ZPETC model-inverse technique [14] to get a stable substitute for the true inverse that can be used in the feedforward controller. The bode plots of the transfer functions $P_{\Omega_e \beta}$, $P_{\Omega_e u}$ and F are shown in Fig. 3, where a 100 Hz sample rate is used. Making the controller causal, the ZPETC requires

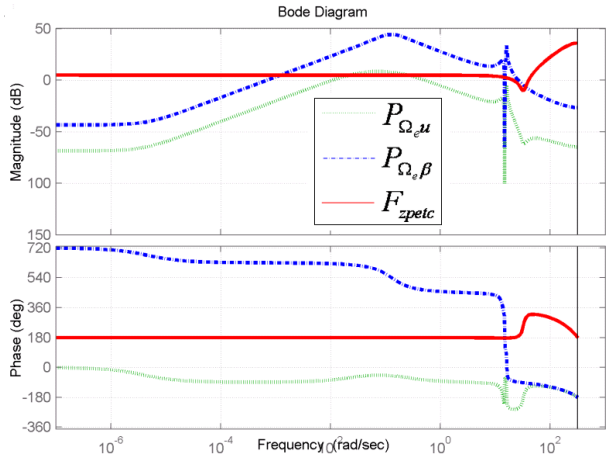

Fig. 3. Bode plots of transfer functions $P_{\Omega_e \beta}$, $P_{\Omega_e u}$ and ZPETC-based feedforward controller F_{zpetc}.

an additional delay of one sample period. Thus, the LIDAR code must provide one sample period preview to cancel this delay, making the phase of this controller match the ideal case exactly.

B. FX-RLS Controller

The LIDAR sensor enables online adjustments to the FX-RLS control law at every time step. In Fig. 4, assume that a perfect wind speed measurement x can be obtained via the

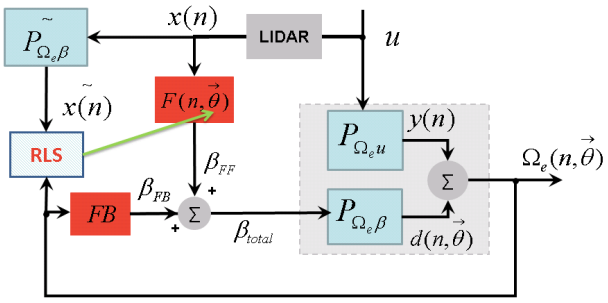

Fig. 4. FX-RLS feedforward control strategy. Two signals are fed into the feedforward controller: the rotor speed error $\Omega_e(n,\vec{\theta})$ and the wind speed measurement upstream to the turbine $x(n)$ obtained from LIDAR sensor.

LIDAR beam sensor, that is, $x = u$. Then, the rotor speed error signal can be expressed by

$$\Omega_e(n,\vec{\theta}) = y(n) + d(n,\vec{\theta}), \tag{3}$$

where n is discrete time step coefficient, $\vec{\theta}$ contains the adaptive feedforward controller parameters, and

$$\begin{aligned} d(n,\vec{\theta}) &= P_{\Omega_e \beta} \cdot (F(n,\vec{\theta}) \cdot x(n) + FB \cdot \Omega_e(n,\vec{\theta})), \\ &= F(n,\vec{\theta}) \cdot P_{\Omega_e \beta} \cdot x(n) + P_{\Omega_e \beta} \cdot FB \cdot \Omega_e(n,\vec{\theta}). \end{aligned}$$

Following the procedure in [15], let

$$\tilde{x(n)} := \tilde{P_{\Omega_e \beta}} \cdot x(n),$$

where $\tilde{P_{\Omega_e \beta}}$ is an approximation of $P_{\Omega_e \beta}$. Thus, the error (3) can be approximated by

$$\Omega_e(n,\vec{\theta}) \approx \frac{y(n) + F(n,\vec{\theta}) \cdot \tilde{x(n)}}{1 - P_{\Omega_e \beta} \cdot FB}. \tag{4}$$

The first control goal is to minimize the rotor speed error signal $\Omega_e(n,\vec{\theta})$ in region 3, that is to find the minimized rotor speed error by adapting the parameters $\vec{\theta}$ of the feedforward controller (5). A secondary goal is load reduction. Also, the denominator of (4) is not a function of $\vec{\theta}$ or n, so the feedback control loop does not affect the optimization problem that determines the adaptive feedforward controller $F(n,\vec{\theta})$:

$$\min_{\theta} \frac{1}{N} \sum_{n=1}^{N} \Omega_e^2(n,\theta) \tag{5}$$

We have selected a finite impulse response (FIR) filter for $F(n,\vec{\theta})$ because of its inherent stability, which is particularly useful for an adaptive control approach [16]. The RLS algorithm computes the coefficients of the FIR adaptive feedforward controller at each time step. The choice of the RLS algorithm's initial conditions influences the performance of the FX-RLS feedforward control strategy, especially early in the simulation and when there is inadequate persistent excitation.

The number of coefficients in the adaptive FIR feedforward controller is selected to obtain the desired preview time based on the LIDAR sampling frequency. We start with LIDAR measurements 70 m in front the hub, which corresponds to 3.9 sec of preview if the wind speed is 18 m/s.

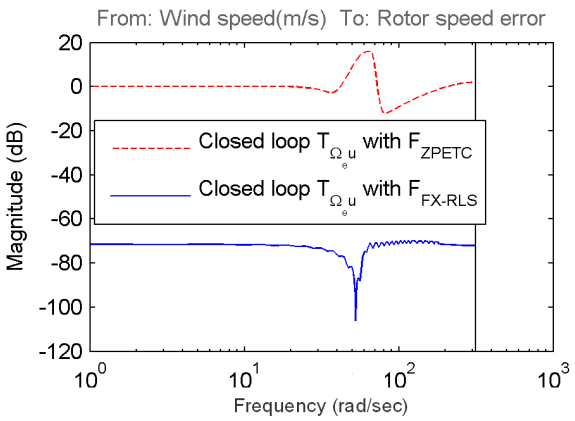

Fig. 5. The magnitude bode plots of the closed loop transfer function $T_{\Omega_e u}$ from the wind speed input u to rotor speed error Ω_e with the two feedforward control techniques (F_{zpetc} and F_{FX-RLS}) designed to mitigate the effect of wind speed disturbances on the rotor speed error.

To construct the RLS algorithm, an approximation of the dynamics $P_{\tilde{\Omega}_e\beta}$ is required to create the filtered signal $x(\tilde{n})$. In [15] and [17], both offline and online system identification techniques for filtered least mean square (FX-LMS) algorithm are applied to obtain this estimation, where an external signal is injected into the system as the excitation signal. In this research, we have studied both offline and online system identification and we use another FIR filter to represent the dynamics of $P_{\tilde{\Omega}_e\beta}$. The offline values of the FIR filter for representing the dynamics of $P_{\tilde{\Omega}_e\beta}$ are simply the steady state coefficient values for one online case test. Because the $P_{\tilde{\Omega}_e\beta}$ is only an approximation, we have also experimented with a simple fixed gain instead of a FIR filter. This gain was selected from the offline filter coefficients to be 0.3163e-006.

Using offline identification for the $P_{\tilde{\Omega}_e\beta}$, we can find a steady state approximation to the FX-RLS-based feedforward controller. The magnitude bode plots of the closed loop transfer functions $T_{\Omega_e u}$ obtained from the two feedforward control techniques (F_{zpetc} and F_{FX-RLS}) combined with PI feedback are shown in Fig 5, where $T_{\Omega_e u}$ maps the wind input u to rotor speed error Ω_e. The steady state FX-RLS feedforward controller rejects the wind disturbance better than the ZPETC feedforward controller.

V. Simulation Results

Our first simulations assume that a perfect wind measurement is obtained from the LIDAR at 100 Hz. Then, we study the effects of different LIDAR data update rates and preview times in the FX-RLS feedforward control. Controller effectiveness is based on damage equivalent loads (DELs), which are calculated using another NREL code according to a rainflow counting algorithm [18]. We examine the tower base fore-aft and side-to-side bending moments, blade flapwise and edgewise bending moments at the blade roots, averaged generator power, rotor speed root mean square (RMS) value, pitch rate RMS value, and pitch angle RMS value.

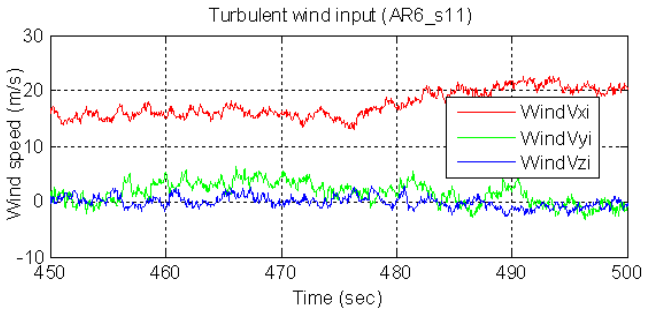

Fig. 6. Turbulent wind field used in simulation. "Wind Vxi" refers to the wind speed in the prevailing direction, "Wind Vyi" refers to the wind speed perpendicular to "Wind Vxi" but parallel to the ground, and "Wind Vzi" is the vertical wind speed.

We note that it is desirable to reduce the tower and blade bending moments, to increase or hold constant the generator power, and to hold constant the rotor speed. Pitch rate is expected to rise as more control actuation is required, but should not rise excessively. Pitch angle should remain within normal operational bounds, which for the CART3 is between about 0-20 deg.

A. Results for 100 Hz LIDAR sampling rate

For the 100 Hz perfect LIDAR measurement case, the FX-RLS feedforward controller uses 1 sec preview time, so the $P_{\Omega_e\beta}$ estimate is a 100 coefficients FIR filter obtained from online system identification. The ZPETC feedforward controller uses one sample period preview time to match the ideal case exactly. The two collective pitch feedforward controllers augment the PI feedback collective pitch controller in a simulation using the turbulent wind field shown in Fig. 6.

The DEL results shown in Fig. 7 are compared to the baseline PI feedback only controller. Simulations run using a LPF to emulate the pitch actuator dynamics with the ZPETC controller showed increased loads compared to simulations with no LPF. Therefore, no LPF is used for either the ZPETC or FX-RLS feedforward controllers in this subsection of results. Fig. 7 shows that the FX-RLS controller outperforms the ZPETC controller with regard to rotor speed tracking and structural load mitigation on the tower and blades. The ZPETC feedforward controller decreases the blade flapwise and edgewise bending moments 7% or less, but worsens the tower fore-aft bending moments and pitch rate by 67.8% and 1971%, respectively, compared with the PI feedback baseline controller.

B. Results for lower LIDAR sampling rates

We next evaluate the FX-RLS strategy with more realistic LIDAR update rates and imperfect wind measurements. Based on the LIDAR unit installed on CART3 at NWTC, we selected 1 Hz and 5 Hz LIDAR update rates and preview times of 1 sec and 4 sec as shown in Table I. The same turbulent wind field is used. Results comparing the FX-RLS algorithm with the baseline in this section include a LPF to emulate the pitch actuator dynamics.

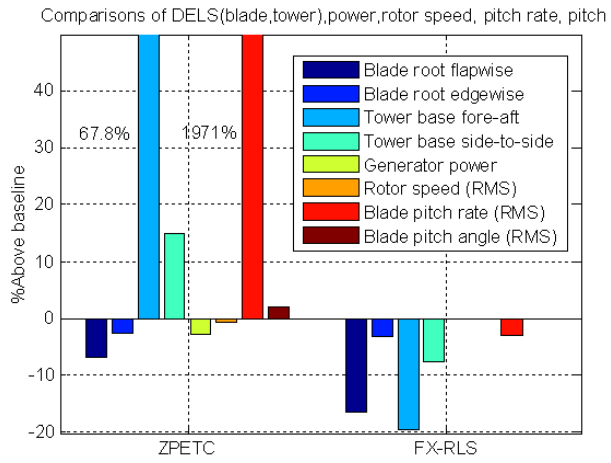

Fig. 7. A comparison of DELs for tower and blade bending moment, averaged generator power, rotor speed RMS value, pitch rate RMS value, and pitch angle RMS value for the ZPETC and FX-RLS feedforward controllers in turbulent wind field, assuming a perfect wind measurements from the 100 Hz LIDAR, compared with the PI feedback baseline controller.

TABLE I

SIMULATED LIDAR UPDATE RATES AND PREVIEW TIME

Case NO.	Preview time [sec]	LIDAR data rate [Hz]	$\tilde{P}_{\Omega\beta}$	Coeffi. # in FF
1	1	100	on-line/100 coeffi. FIR	100
2	1	5	off-line/100 coeffi. FIR	5
3	1	1	off-line/100 coeffi. FIR	1
4	4	1	off-line/100 coeffi. FIR	4
5	4	1	Fix gain	4

Using 1 Hz and 5 Hz LIDAR update rates, we were unable to obtain any satisfactory results when using online system identification for approximating $P_{\Omega_e\beta}$, possibly due to the time-varying nature of the wind input and lower LIDAR sampling rate. Therefore, offline system identification is used. For the 4 sec preview time and 1 Hz LIDAR update rate, using a simple constant scalar gain for the estimation of $P_{\Omega_e\beta}$ is also considered.

Some of the results using 1 Hz and 5 Hz LIDAR update rates and 1 sec and 4 sec preview times are shown in Fig. 8 and Fig. 9. Between 470 sec and 475 sec, the baseline controller allows a large rotor speed overshoot, while the FX-RLS feedforward algorithm mitigates the overshoot by starting to pitch the blades prior to the gust hitting the turbine. Structural loads are also reduced, but the generator power dips.

The overall improvement based on the FX-RLS feedforward controller compared to the baseline with turbulent wind input and Table I cases is shown in the DELs in Fig. 10. The FX-RLS controller decreases both the tower and blade bending moments for all LIDAR measurement rates and preview times shown. According to Fig. 10, with the realistic 1 Hz LIDAR update rate and 4 sec preview time, using offline identification for $P_{\Omega_e\beta}$ estimate, the tower fore-aft and the blade flapwise bending moment can be reduced by almost 12.1% and 15.2%, respectively. When one scalar constant gain is used to estimate $P_{\Omega_e\beta}$, the results are improved

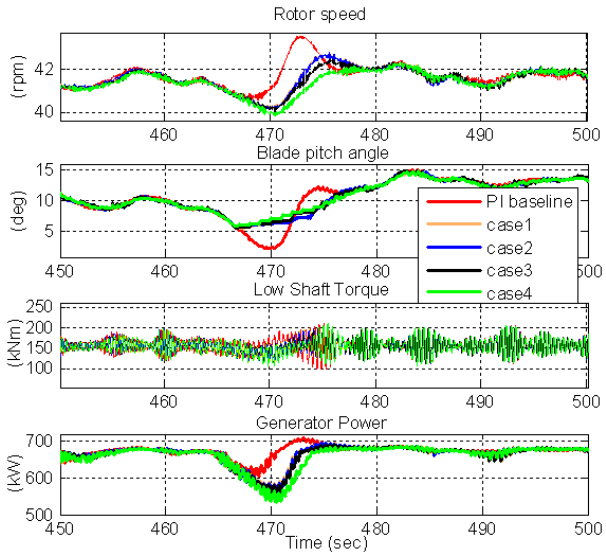

Fig. 8. Time series comparisons of rotor speed, blade pitch angle, low speed shaft torque, and generator power for the cases listed in Table I with turbulent wind input. The FX-RLS feedforward controller improves performance compared to the baseline.

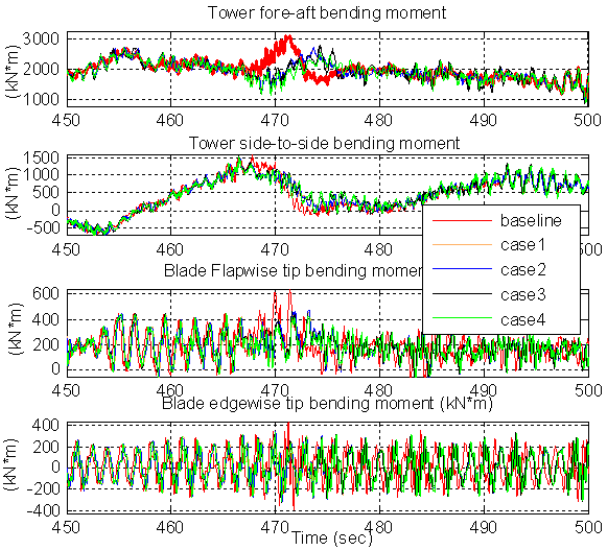

Fig. 9. Time series comparisons of tower fore-aft and side-to-side bending moment and blade flapwise and edgewise bending moment for the cases listed in Table I with turbulent wind input. Performance for the FX-RLS controller is improved compared to the baseline.

compared to the offline case, with the tower fore-aft bending reduced by a magnitude of 20.6% and the blade flapwise bending by 15.1%. Only a 3.8% increase in pitch rate is necessary to achieve these benefits.

VI. CONCLUSION AND FUTURE WORK

In this paper we have described a FX-RLS and a ZPETC feedforward collective blade pitch controller, both of which are combined with a baseline PI feedback controller and designed for structure load mitigation and rotor speed regulation when wind turbine is operating above rated wind speed. Feedforward control is enabled by a LIDAR, and

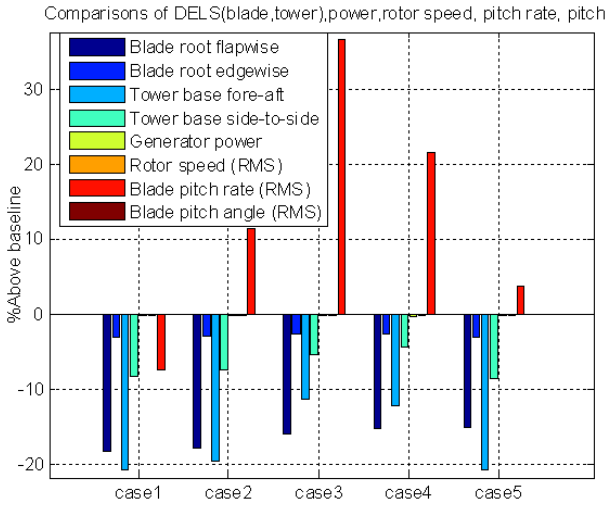

Fig. 10. A comparison of DELs for tower and blade bending moments, averaged generator power, rotor speed RMS value, pitch rate RMS value, and pitch angle RMS value for the FX-RLS feedforward control with different LIDAR update rates and preview time shown in Table I using a realistic turbulent wind input. Compared to the PI feedback only baseline, loads are generally reduced with some tradeoff in blade pitch rate but minimal power loss.

different LIDAR data update rates are used in evaluating these feedforward controllers.

Assuming an accurate and fast LIDAR wind measurement can be obtained, the FX-RLS algorithm-based adaptive feedforward control performed better than the ZPETC model-inverse-based non-adaptive feedforward control. The FX-RLS controller was able to improve the tower and blade bending moments, and pitch rate without much drop in power production. However, the ZPETC controller improved the blade bending moments but worsened the tower loads and pitch rate significantly.

The FX-RLS feedforward controller gave promising performance when realistic 1 Hz and 5 Hz LIDAR update rates were used, as well. For the case most closely resembling expected field conditions at the NWTC, the adaptive feedforward was able to improve the tower fore-aft bending moment by 20.6% and blade flapwise bending moment by 15.2%. The power production decreased by less than 0.3% and an increase in pitch rate of less than 4%.

Future work will include a more realistic LIDAR model, different types of LIDAR units, and the use of LIDAR-enabled feedforward control when the wind turbine is operating below rated wind speed.

REFERENCES

[1] A. Wright, *Modern Control Design for Flexible Wind Turbines*. Golden, CO: National Renewable Energy Laboratory, 2004.

[2] K. Stol and M. Balas, "Periodic disturbance accommodating control for blade load mitigation in wind turbines," in *ASME J. Solar Energy Engineering*, vol. 125(4), pp. 379–385, 2003.

[3] M. H. Hansen, A. Hansen, and T. J. L. etc., *Control design for a pitch-regulated, variable speed wind turbine*. Roskilde, Denmark: Riso National Laboratory, January 2005.

[4] J. Jonkman, S. Butterfield, W. Musial, and G. Scott, "Definition of a 5-mw reference wind turbine for offshore system development," in *NREL/TP-500-38060*, Feb. 2009.

[5] T. Mikkelsen, K. Hansen, N. Angelou, M. Sjoholm, M. Harris, P. Hadley, R. Scullion, and G. Ellis, "Lidar wind speed measurements from a rotating spinner," in *European Wind Energy Conference and Exhibition*, (Poland,Warsaw), April 2010.

[6] F. Dunne, L. Y. Pao, A. D. Wright, B. Jonkman, and N. Kelley, "Combining standard feedback controllers with feedforward blade pitch control for load mitigation in wind turbines," in *Proceedings of American Institute of Aeronautics and Astronautics*, 2010.

[7] J. Zeng, B. Moulin, R. de Callafon, and M. Brenner, "Adaptive feedforward control for gust loads alleviation," in *Proc. AIAA Atmospheric Flight Mechanics Conf.*, (Honolulu, HI), Aug 2008.

[8] M. Tomizuka, "Zero phase error tracking algorithm for digital control," in *ASME Journal of Dynamic Systems*, vol. 109, pp. 65–68, 1987.

[9] P. Fleming, J. van Wingerden, A. Wright, and L. Fingersh, "Resonant vibrations resulting from the re-engineering of a constant-speed 2-bladed turbine to a variable-speed 3-bladed turbine," in *49th AIAA Aerospace Sciences Meeting*, (Orlando, Florida), Jan.4-7 2011.

[10] K. E. Johnson, L. Y. Pao, M. J. Balas, and L. J. Fingersh, "Control of variable-speed wind turbines: Standard and adaptive techniques for maximizing energy capture," *IEEE Control Systems Magazine*, vol. 26, pp. 70–81, June 2006.

[11] J. Jonkman and M. L. Buhl, *FAST User's Guide*. Golden, CO: National Renewable Energy Laboratory, 2005.

[12] E. Simley, L. Y. Pao, R. Frehlich, B. Jonkman, and N. Kelley, "Analysis of wind speed measurements using coherent lidar for wind preview control," in *Proceedings of American Institute of Aeronautics and Astronautics*, 2011.

[13] N. D. Kelley and B. J. Jonkman, *Overview of the Turbsim Stochastic Inflow Turbulence Simulator: Version 1.21 (Revised Feb. 1, 2007)*. Golden, CO: National Renewable Energy Laboratory, April 2007.

[14] T. Masayoshi, "Zero phase error tracking algorithm for digital control," in *Jounal of Dynamic System, Measurement, and Control*, vol. 109, March 1987.

[15] J. Zeng and B. Moulin, "Adaptive feedforward control for gust load alleviation," in *Journal of Guidance, control, and dynamics*, vol. 33, pp. 862–872, 2010.

[16] J.S.Vipperman and R.A.Burdisso, "Adaptive feedforward control of non-minimum phase structural systems," in *Journal of Sound and Vibration*, vol. 183(3), pp. 369–382, 1995.

[17] M. T. Akhtar, M. Abe, and M. Kawamata, "Modified-filtered-x lms algorithm based active noise control systems with improved online secondary-path modeling," in *Proc. IEEE Int. Midwest Symp. on Circuits Systems*, vol. 1, pp. 13–16, 2004.

[18] S. D. Downing and D. F. Socie, "Simple rainflow counting algorithms," in *Journal of Communication and Computer*, vol. 4, pp. 31–40, Jan 1982.